ChemComm

Accepted Manuscript

This article can be cited before page numbers have been issued, to do this please use: Z. Xu, P. Zhang, Y. Chai, H. Wang and R. Yuan, *Chem. Commun.*, 2018, DOI: 10.1039/C8CC04953J.

This is an Accepted Manuscript, which has been through the Royal Society of Chemistry peer review process and has been accepted for publication.

Accepted Manuscripts are published online shortly after acceptance, before technical editing, formatting and proof reading. Using this free service, authors can make their results available to the community, in citable form, before we publish the edited article. We will replace this Accepted Manuscript with the edited and formatted Advance Article as soon as it is available.

You can find more information about Accepted Manuscripts in the author guidelines.

Please note that technical editing may introduce minor changes to the text and/or graphics, which may alter content. The journal's standard Terms & Conditions and the ethical guidelines, outlined in our author and reviewer resource centre, still apply. In no event shall the Royal Society of Chemistry be held responsible for any errors or omissions in this Accepted Manuscript or any consequences arising from the use of any information it contains.

View Article Online
DOI: 10.1039/C8CC04953J

Journal Name

COMMUNICATION

A Biosensor Based on 3D-DNA Walking Machine Network and Distance-controlled Electrochemiluminescence Energy Transfer for Ultrasensitive Detection of Tenascin C and Lead Ion

Received 00th January 20xx,
Accepted 00th January 20xx

DOI: 10.1039/x0xx00000x

www.rsc.org/

Zi-Qi Xu, Pu Zhang, Ya-Qin Chai, Hai-Jun Wang*, Ruo Yuan*

An electrochemiluminescence biosensor was proposed based on distance-controlled energy transfer and 3D-DNA walking machine network for significantly improving the mass transport, offering an ultrasensitive and controllable strategy for different types of targets detection.

DNA walking machine, the fabricated molecular machine produced by intelligent synthetic DNAs which controlled actions accurately and performed tasks efficiently, has received wide attention.[1-5] However, comparing with the traditional DNA walking machines constructed by one dimensional (1D) or two dimensional (2D) tracks with low DNA local concentration, three dimensional (3D) DNA walking machine stood out for its higher walking efficiency and better signal amplification efficiency.[6-9] For example, Ji and co-workers proposed a biosensor with independent 3D-DNA walking machine assembled on the sensing platform for thrombin detection.[10] Most recently, our previous work reported an electrochemiluminescence (ECL) biosensor for microRNA analysis with using independent 3D-DNA walking machine.[11] Although the above strategies realized target detection, the performances of these biosensors were limited because of the restricted loading capacity of the independent 3D-DNA walking machines. In this paper, we proposed to construct a 3D-DNA walking machine network through the hybridization of two DNA linkers assembled on different 3D-DNA walking machines. On account of the excellent loading capacity of the network structure, this strategy was of importance in significantly improving the loading capacity of 3D-DNA walking machines for further increasing the sensitivity of biosensor.

Multi-target detection strategy has become a hotspot in biosensing, which reflects more comprehensive information and is significant for monitoring and therapeutics of diseases.[12-14] For example, Jiang's group constructed a potential-resolution strategy to detect two antigens at the cell surface.[15] However, the system required to label diverse ECL luminophores on the DNA probes and had cross-reactivity between the luminophores. To overcome this problem, our group recently applied multivariate linear algebraic equations to realize the detection of multiple proteins.[16] Unfortunately, the method required abundant laboratory data and the establishment of complex mathematical models. In addition, TNC is highly expressed in solid tumors such as glioma and breast cancer, and the expression intensity was related to tumor grade.[17,18] Lead ions (Pb^{2+}), the highly toxic heavy metal pollutant which seriously threatened to human health, played a tumor promoting effect in tumors including lung tumor and renal tumor,[19,20] and might be associated with TNC to the same disease. As far as we know, no studies have been reported for determination of TNC and Pb^{2+} in one system. Therefore, it is an urgent challenge to develop a simple and feasible strategy to overcome the cross reaction of diverse luminophores and the tedious operation of data processing for multiple targets detections of TNC and Pb^{2+}.

Key Laboratory on Luminescence and Real-Time Analytical Chemistry, Ministry of Education, School of Chemistry and Chemical Engineering, Southwest University, Chongqing 400715, People's Republic of China.
E-mail: hjwang@swu.edu.cn; yuanruo@swu.edu.cn.
Tel.: +86-23-68252277; Fax.: +86-23-68253172.
Electronic supplementary information (ESI) available: Experimental details and additional figures. See DOI: 10.1039/x0xx00000x

View Article Online
DOI: 10.1039/C8CC04953J

Herein, we proposed a novel biosensor based on 3D-DNA walking machine network and distance-controlled ECL energy transfer for TNC and Pb^{2+} detection. Firstly, AuNPs@Fe_3O_4 with relatively large specific surface area was immobilized with CdS:Mn QDs modified hairpin DNA S1 (CdS:Mn-S1), first antibody-labeled DNA W1 (Ab1-W1) and one DNA linker (H1 or H2) for the formation of 3D-DNA walking machine. Then, the network nanostructure was assembled by the hybridization of

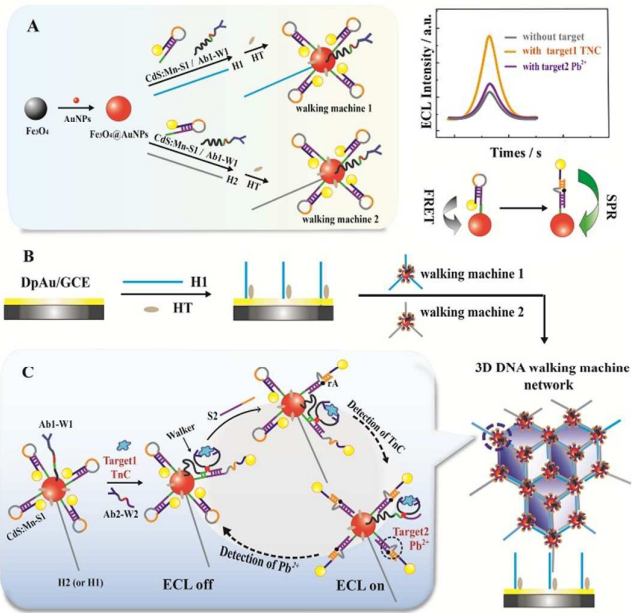

Scheme 1 The preparation of two kinds of 3D-DNA walking machine (A), the construction of the ECL biosensor based on 3D-DNA walking machine network (B) and the detection mechanism of target TNC and Pb^{2+} (C).

two DNA linkers (H1 and H2 immobilized on different 3D-DNA walking machine), which significantly improved the loading efficiency of 3D-DNA walking machine. Then, inspired by target-induced DNA structural switching,[21,22] multi-target detection was realized based on the obtained network nanostructure. At the initial state, the hairpin structure of S1 made CdS:Mn QDs close to AuNPs, resulting in a weak ECL response in account of Förster energy transfer (FRET, ''off'' state). Then, the presence of target 1 TNC induced the specific combination of Ab1-W1 and Ab2-W2 to serve as walker for opening the hairpin DNA S1. Later, DNA S2 fully hybridized with S1 to obtain S1-S2 double-strands DNA (dsDNA) with a recognition site of Pb^{2+}, liberating the walker to hybridize with another S1. Simultaneously, the obtained S1-S2 dsDNA could compel CdS:Mn QDs away from Au nanoparticle (AuNP), which generated an enhanced ECL for TNC detection due to the excited surface plasma resonance (SPR, ''on'' state). Subsequently, S2 was cleaved by target 2 Pb^{2+} to restore the hairpin structure of S1 for closing AuNP and CdS:Mn QDs, decreasing the ECL signal for Pb^{2+} detection in account of FRET. ("off" state). Thus, the proposed biosensor achieved ultrasensitive detection of different types of targets with the detection limit for TNC of 36.8 ag mL^{-1} and Pb^{2+} of 0.8 fg mL^{-1}. To sum up, the high loading efficiency of 3D-DNA walking machine network strategy not only widen the application of 3D-DNA walking machine in biosensing, but also offered an ultrasensitive and controllable method for different types of targets detection.

The synthesis of nanomaterials including Ab1-W1, Ab2-W2, AuNPs@Fe_3O_4, CdS:Mn-S1 and two kinds of 3D-DNA walking machine were detailed description in the supplementary material. Besides, the morphology of AuNPs and CdS:Mn QDs were characterized by transmission electron microscope (TEM, ESI† Fig. S1 A) and high resolution transmission electron microscopy (HRTEM, ESI† Fig. S1 B) respectively. And the ECL emission spectra of CdS:Mn QDs and UV-vis absorption spectra of AuNPs were also studied for proving the energy transfer of AuNPs/CdS:Mn QDs system (ESI† Fig. S1 C).

To confirm the "off-on-off" stages of the system, the stepwise fabrication of this biosensor was examined by ECL measurements. (see ESI† for experimental details). As shown in Figure 1 A, firstly, the CdS:Mn QDs on the DNA walking machine network were close to AuNPs, providing a weak ECL signal due to FRET (curve a, "off" state). Later, the addition of target TNC and S2 resulted in a strong ECL signal (curve b). Considering that target TNC could bind with Ab1-W1 and Ab2-W2 to generate walker, increasing the distance between CdS:Mn QDs and AuNPs and resulted in a strong ECL signal ("on" state). Finally, the introduction of Pb^{2+} lead to a decreased ECL signal (curve c) which had the similar value as

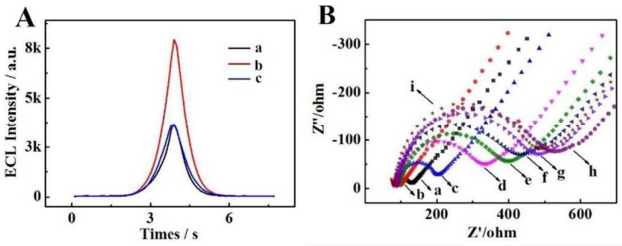

Figure 1 (A) ECL response of the biosensor successively incubated with 3D-DNA walking machine network (off state, curve a), 100 fg mL^{-1} target TNC and S2 (on state, curve b), 100 fg mL^{-1} target TNC, S2 and 1 μM Pb^{2+} (off state, curve c). (B) EIS diagram of the biosensor assembly process. (a) GCE, (b) GCE/DpAu, (c) GCE/DpAu/H1, (d) GCE/DpAu/H1/HT, (e) GCE/DpAu/H1/HT/two kinds of DNA walking machine, (f) GCE/DpAu/H1/HT//two kinds of DNA walking machine/TNC, (g) GCE/DpAu/H1/HT//two kinds of DNA walking machine/TNC/Ab2-W2, (h) GCE/DpAu/H1/HT//two kinds of DNA walking machine/TNC/Ab2-W2/S2 (i) GCE/DpAu/H1/HT//two kinds of DNA walking machine/TNC/Ab2-W2/S2/Pb^{2+}.

curve a. Thus because the Pb^{2+} cut off S2 to restore the hairpin structure of S1, which closed the distance between AuNPs and CdS:Mn QDs to quench the ECL signal ("off" state). All the results suggested the feasibility of the "off-on-off" stages of the biosensor.

For validating the successful preparation of the proposed biosensor, electrochemical impedance spectroscopy (EIS) was employed and the results were classified as Figure 1 B. Firstly, the AuNPs with superior electronic conductivity were electrodeposited on the electrode surface (curve b), leading to a decreased electron transfer resistance (R_{et}) than that of the bare GCE (curve a). Then H1 was incubated on the sensing surface, resulting in an increased R_{et} (curve c) which was attributed to the fact that DNA with the negatively charged

View Article Online
DOI: 10.1039/C8CC04953J

phosphate backbone would attenuate the electron transfer. And then, HT with insulating properties was used to block the nonspecific sites, which led to an increased R_{et} (curve d). As expected, an increasing R_{et} could be observed after the introduction of two kinds of DNA walking machine due to the negatively charged phosphate backbone from numerous DNA, suggesting the successful assembly of 3D-DNA walking machine network (curve e). Then, TNC and Ab2-W2 were incubated in turn and the increased R_{et} were observed due to their insulating properties (curve f and curve g). Later, the addition of S2 resulted in an increased R_{et}. Finally, after the addition of Pb^{2+}, a decreased R_{et} was observed due to the releasing of DNA segments from sensing surface after the specific cleavage of Pb^{2+}. These results suggested the successful preparation of the biosensor.

For exploring the quantitative application of this method, the biosensor was employed for target TNC and Pb^{2+} detection under the optimal conditions (see ESI†). As seen in Figure 2 A, with increasing concentrations of TNC from 100 ag mL^{-1} to 1 ng mL^{-1}, the ECL signals were increased correspondingly and linearly responded to the logarithms of TNC concentration with a regression equation of I_1 = 9722.79 + 1292.77 lg c_1 and correlation coefficient was 0.9989 (I_1 stands for ECL intensity and c_1 stands for the concentration of TNC). And the evaluated detection limit was 36.8 ag mL^{-1}. As for Pb^{2+} detection, the

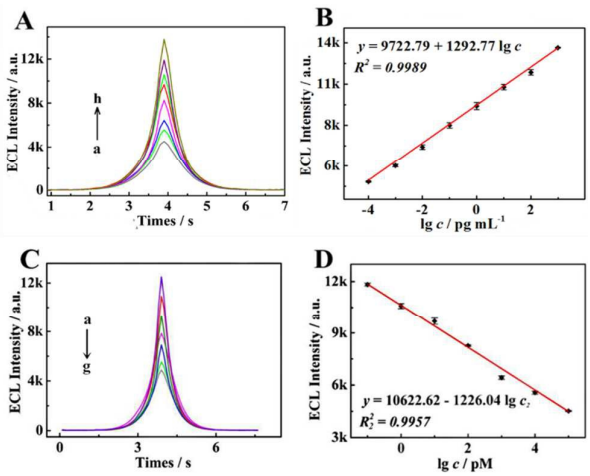

Figure 2 (A) ECL response of biosensor incubated with different concentrations of TNC: a. 100 ag mL^{-1}, b. 1 fg mL^{-1}, c. 10 fg mL^{-1}, d. 100 fg mL^{-1}, e. 1 pg mL^{-1}, f. 10 pg mL^{-1}, g. 100 pg mL^{-1}, h. 1 ng mL^{-1}. (B) The calibration curves of TNC analysis. (C) ECL response of biosensor with different concentrations of Pb^{2+}: a. 2 fg mL^{-1}, 20 fg mL^{-1}, b. 200 fg mL^{-1}, c. 2 pg mL^{-1}, d. 20 pg mL^{-1}, e. 200 pg mL^{-1}, f. 2 ng mL^{-1}. (D) The calibration curves of Pb^{2+} analysis.

designed biosensor also had an outstanding performance. As seen from Figure 2 C, when the concentrations of Pb^{2+} increased from 2 fg mL^{-1} to 2 ng mL^{-1}, the ECL signals were decreased gradually and the decreasing degree of the ECL signals was linearly responded to the logarithms of Pb^{2+} concentration with a regression equation of I_2 = 10622.62–1226.04 lg c_2 (I_2 stands for ECL intensity and c_2 stands for the concentration of Pb^{2+}). The correlation coefficient was 0.9957 and evaluated detection limit was 0.8 fg mL^{-1}. Compared with the existing detection methods (see ESI† Table S2), the well-designed biosensor not only realized different types of target detection, but also showed higher sensitivity toward target analysis, suggesting a promising perspective of the proposed 3D-DNA nanomachine network in clinical diagnosis and bioapplication.

Stability was an important factor in evaluating the performance of biosensors. As shown in Figure 3 A, the ECL responses of the biosensor incubated with 10 pg mL^{-1} TNC (curve a) and 2 ng mL^{-1} Pb^{2+} (curve b) appeared no evident differences under consecutive scanning of 16 cycles, which showed a satisfied stability of the ECL biosensor. And the reproducibility of the designed biosensor was also studied by evaluating the coefficient of variation (ECL signal) of three repeated measurements with a relative standard deviation (RSD) of less than 5%. Besides, the interfering agents including proteins mucin 1 (MUC1) and cardiac troponin T antigen (cTnT) were examined to assess the selectivity of the developed biosensor. As we can see in Figure 3 B, an effectively enhanced

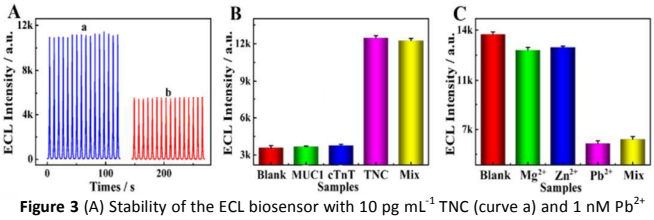

Figure 3 (A) Stability of the ECL biosensor with 10 pg mL^{-1} TNC (curve a) and 1 nM Pb^{2+} (curve b) under 16 cycles scanning. (B) Selectivity of the ECL biosensor towards target TNC detection (blank, 1 ng mL^{-1} MUC1, 1 ng mL^{-1} cTnT, 100 pg mL^{-1} target TNC and a mixture of 1 ng mL^{-1} MUC1, 1 ng mL^{-1} cTnT and 100 pg mL^{-1} target TNC). (C) Selectivity of the ECL biosensor towards target Pb^{2+} detection (blank, 100 nM Mg^{2+}, 100 nM Zn^{2+}, 1 nM Pb^{2+} and a mixture contained 100 nM Mg^{2+}, 100 nM Zn^{2+} and 1 nM Pb^{2+}).

ECL intensity was appeared when TNC was added both in the pure target solution and the mixture solution. However, the ECL intensities of the biosensors incubated with MUC1 or cTnT did no obvious enhancement in comparison with the blank reagent, which indicated remarkable specificity of the biosensor for TNC detection. Consequently, the relevant ion such as Zn^{2+} and Mg^{2+} were employed to verify the selectivity of Pb^{2+} detection. As shown in Figure 3 C, both the blank sample and the Zn^{2+}, Mg^{2+} samples showed a high ECL signal. But when the target Pb^{2+} or the mixture containing Pb^{2+} were incubated, the ECL signal decreased sharply which indicated the specific response of the biosensor for Pb^{2+} detection. The above consequences indicated that our proposed ECL biosensor possessed outstanding performances. Moreover, for investigating the practical application of this system, the biosensor was employed in real samples for target TNC detection (see ESI† Table S3).

Conclusions

In conclusion, a novel biosensor was constructed based on 3D-DNA walking machine network and distance-controlled ECL energy transfer for TNC and Pb^{2+} detection. The main features and advantages were listed as follows. Firstly, our study presented a new method of 3D-DNA walking machine network through simple base pairing between DNA linkers, which

View Article Online
DOI: 10.1039/C8CC04953J

significantly improved the loading efficiency of nanomachines and the sensitivity of the biosensor. Secondly, the biosensor achieved different types of targets detection in account of distance-controlled ECL energy transfer between AuNPs and CdS:Mn QDs, which was of great significance in clinical diagnosis. Comparing with the traditional DNA walking machine, the proposed DNA walking machine network enabled the biosensor to detect with different target with ultrasensitivity, which paved a promising avenue of the DNA nanodevices in the wide application of clinical diagnosis.

Conflicts of interest

There are no conflicts to declare.

Acknowledgement

This work was financially supported by the National Natural Science Foundation of China (21775124, 51473136, 21575116 and 21675129), Fundamental Research Funds for the Central Universities (XDJK2017C023), Chongqing Postdoctoral Science Foundation (Xm2017016), the Natural Science Foundation Project of CQ CSTC (cstc2017jcyjA1305) and China - Singapore Plan (Chongqing).

Notes and references

1 X. M. Qu, D. Zhu, G. B. Yao, S. Su, J. Chao, H. J. Liu, X. L. Zuo, L H. Wang, J. Y. Shi, L. H. Wang, W. Huang, H. Pei, C. H. Fan, *Angew. Chem. Int .Ed.,* 2017, **56**, 1855-1858.
2 C. Jung, P. B. Allen, A. D. Ellington, *Nature Nanotech*., 2016, **11**, 157-163.
3 M. H. Liu, J. L. Fu, C. Hejesen, Y. H. Yang, N. W. Woodbury, K. Gothelf, L. Yan, H. Yan, *Nat. Commun*., 2013, **4**, 2127.
4 N. X. Li, J. Zheng, C. R. Li, X. X. Wang, X. H. Ji, Z. K. He, *Chem. Commun.,* 2017, **53**, 8486-8488.
5. J. Pan, F. Li, T. G. Cha, H. Chen, J. H. Choi, *Current Opinion in Biotechnology*, 2015, **34**, 56-64.
6 W. Li, L. Wang, W. Jiang. *Chem. Commun.* 2017, **53**, 5527-5530.
7 X. L. Yang, Y. A. Tang, S. D. Mason, J. B. Chen, F. Li, *ACS Nano,* 2016, **10**, 2324-2330.
8 Y. Y. Yang, M. A. Goetzfried, K. Hidaka, M. X. You, W. H. Tan, H. Sugiyama, M. Endo, *Nano Lett*., 2015, **10**, 6672-6676.
9 J. L. Liu, Z. L. Tang, J. Q. Zhang, Y. Q. Chai, R. Yuan, *Anal. Chem*., 2018, **90**, 5298-5305.
10 Y. H. Ji, L. Zhang, L. Y. Zhu, J. P. Lei, J. Wu, H. X. Ju, *Biosens. Bioelectron*, 2017, **96**, 201-205.
11 Z. Q. Xu, L. L. Liao, Y. Q. Chai, H. J. Wang, R. Yuan, *Anal. Chem*., 2017, **89**, 8282-8287.
12 M. J. Hsu, Yi. H. Chen, *Stat. Med*., 2016, **35**, 202-213.
13 M. Y. Yang, Y. Li, Y. Y. Huai, C. Y. Wang, W. F. Yid, C. B. Mao, *Chem. Commun.,* 2018, **54**, 1631-1634.
14 Y. Jing, Q. Cao, L. Hao, G. G. Yang, W. L. Hu, L. N. Ji, Z. W. Mao, *Chem. Commun.,* 2018, **54**, 271-274.
15 F. F. Han, H. Jiang, D. J. Fang, D. C. Jiang, *Anal. Chem*., 2014, **86**, 6896-6902.
16 W. B. Liang, C. Fan, Y. Zhuo, Y. N. Zheng, C. Y. Xiong, Y. Q. Chai, R. Yuan, *Anal. Chem*., 2016, **88**, 4940-4948.
17 G. Orend, R. Chiquet-Ehrismann, *Cancer Lett.*, 2006, **244**, 143-163.
18 R. Chiquet-Ehrismann, M. Chiquet, *J. Pathol*., 2003, **200**, 488- 499.
19 J. Singh, D. E. Pritchard, D. L. Carlisle, J. A. Mclean, A. Montaser, J. M. Orenstein, S. R. Patierno, *Toxicol. Appl. Pharm*., 1999, **161**, 240-248.
20 Z. Elias, O. Poirot, F. Baruthio, M. C. Daniere, *Carcinogenesis*, 1991, **12**, 1811-1816.
21. G. Liu, Y. Wan, V. Gau, J. Zhang, L. H. Wang, S. P. Song, C. H. Fan, *J. Am. Chem. Soc.,* 2008, **130**, 6820-6825.
22. D. Li, S. P. Song, C. H. Fan, *Acc. Chem. Res.,* 2010, **43**, 631-641.